Unsteady Buoyancy-Induced and Turbulent Flow from a Hot Horizontal Jet Entrance into a Solar Water Storage

M.F. EL-AMIN
Department of Mathematics, Aswan Faculty of Science
South Valley University
EGYPT

W. HEIDEMANN AND H. MUELLER-STEINHAGEN
Institute of Thermodynamics and Thermal Technology (ITW)
University of Stuttgart
Pfaffenwaldring 6 D-70550 Stuttgart
GERMANY

Abstract:- Experimental visualizations and numerical CFD calculations of a horizontal hot water jet entering cold water into a rectangular storage tank are described. Three different temperature differences and their corresponding Reynolds numbers are considered. Both experimental visualization and numerical calculations are carried out for the same flow and thermal conditions. The realizable $k-\varepsilon$ model is used for modeling the turbulent flow while the buoyancy is modeled using a Boussinesq approximation. Polynomial approximation of the water properties are used to compare with the Boussinesq approximation. Numerical solutions are obtained for unsteady flow while pressure, velocity, temperature and turbulence distributions inside the water tank as well as Froude number are analyzed. The experimental visualizations are performed at intervals of five seconds for all different cases. The simulated results are compared with the visualized results, and both of them show the stratification phenomena and buoyancy force effects due to temperature difference and density variation. After certain times, depending on the case condition, the flow tends to reach a steady-state.

Key-words:- Turbulent flow, realizable $k-\varepsilon$ turbulence model, unsteady flow, heat transfer, jet, solar storage, CFD, flow visualization.

1 Introduction

Thermal stratification in the storage tanks has a strong influence on the thermal performance of solar heating systems. The water entering the solar water storage as a jet causes mixing which destroys the stratifications. CFD-software has been used widely to simulate the components of solar heating systems. Cabelli [1] and Knudsen et al. [2] studied the effect of thermal stratification phenomena in the storage tank by means of experiments and numerical computation. They concluded that the effect of thermal stratification in storage tanks is very important for the thermal performance. Shah and Furbo [3] presented a numerical and experimental analysis of water jets entering a solar storage tank. Three inlet designs with different inlet flow rates were simulated out to illustrate the varying behavior of the thermal conditions in a solar store. Their results showed how the inlet design influences the flow patterns in the tank and how the energy quality in a hot water tank is reduced with a poor inlet design. Velocity and temperature fields around a cold water inlet device of small solar domestic hot water tanks were investigated by Jordan and Furbo [4] using the CFD tool Fluent. The simulation results were compared with temperature measurements inside a commercial storage tank. Knudsen et al. [5] analyzed the flow structure and heat transfer in a vertical mantle heat exchanger. The flow structure and velocities in the inner tank and in the mantle were measured using a Particle Image Velocimetry (PIV) system.

This paper introduces an analysis for three temperature differences with the three corresponding Reynolds numbers of horizontal hot water jets entering a rectangular solar storage tank filled with cold water. In order to investigate the stratification phenomena inside the tank, an

experimental visualization was performed for the different cases in sequential time steps, followed by numerical investigations for the same conditions with wide-ranging of analyses for fields of pressure, velocity, temperature and turbulence inside the water store.

2 Experimental Flow Visualizations

Visualization has been used to observe the flow patterns and thermal effects in a solar storage tank with dimensions in meter $X \times Y \times Z = 0.486 \times 0.275 \times 0.29$. Outflow of the tank is on the top, i.e. there is no cover for the tank. In Fig. 1 a systematic diagram for the problem is drawn. Red dye is applied to visualize the charging process of the tank. The colored hot water enters the tank through a horizontal inlet nozzle which has a diameter of 0.007 m.

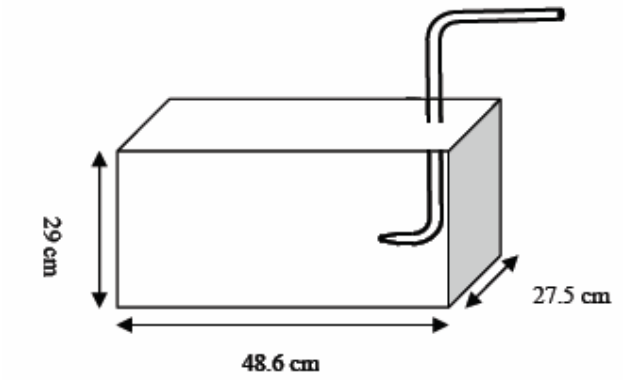

Fig. 1: Sketch of the water tank

The parameters which are used for the three case of studies are entered in Table 1, where Re is the Reynolds number, T_{cold} is the temperature of the water in the tank at the beginning of the experiment, T_{in} is the temperature of the entering water, $\Delta T = T_{in} - T_{cold}$ is the temperature difference between the hot water and the cold water and t is the total time of the visualization. For the three cases, the flow rate is 0.7 l/min and the velocity inlet is 0.3 m/sec. Visualizations are performed by using a digital video camera every five seconds. Fig. 2 shows an example of visualization for the flow patterns during a draw-off test with an inlet flow rate of 0.7 l/min with three different inlet temperatures for the three cases. The buoyancy effects due to natural convection are clearly illustrated in Fig. 2, such that for the isothermal case ($\Delta T = 0$), there is no buoyancy effect because there is no heat transfer, while for the second and third case it can be observed that the red colored water (hot water) moves to the top of the tank depending on the temperature difference. Also, one can note that the buoyancy force of the third case $\Delta T = 40\ K$ is greater than of the second case $\Delta T = 20\ K$.

Table 1: Overview of the experiments

-case	Re	T_{cold}	T_{in}	ΔT	time
First	2100	20	20	0	95 sec
Second	3200	19	40	21	85 sec
Third	4400	21	60	39	105 sec

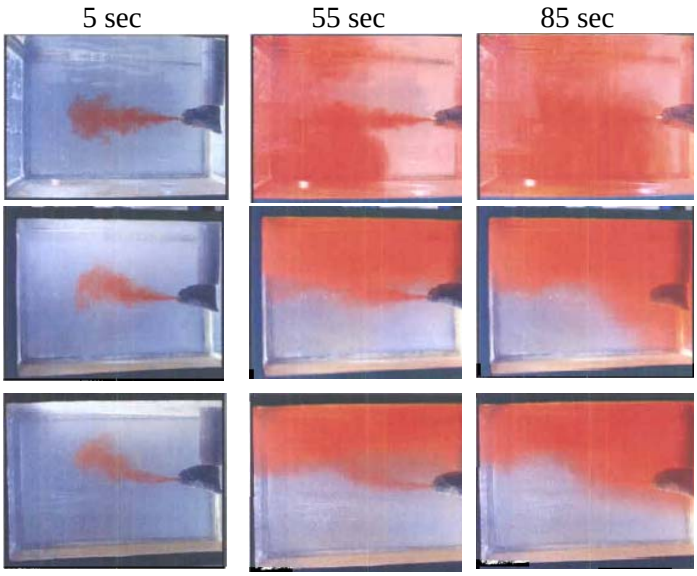

Fig. 2: Visualization of flow structures for $\Delta T = 0$ (1^{st} row), $\Delta T = 20$ (2^{nd} row) and $\Delta T = 40$ (3^{rd} row).

3 Numerical Investigations

The problem of a 3-D horizontal hot water jet entering cold water in a rectangular storage tank is considered. The Reynolds-averaged Navier-Stokes (RANS) equations with the realizable $k-\varepsilon$ model which was suggested by Shih et al. [6] is used for modeling of the turbulent flow while the buoyancy is modeled by Boussinesq buoyancy approximation. The realizable $k-\varepsilon$ model was originally proposed by Reynolds [7]

The current problem is to visualize and to simulate the stratification of the hot water inside a water store. Symmetry is assumed in the vertical central plane of the tank, so for this model only half

of the tank is modeled. Fig. 3 shows the model outline for the symmetrical half tank with the dimensions $X \times Y \times Z = 0.486 \times 0.1375 \times 0.29\, m$. Furthermore, heat transfer through the walls of tank is not taken into consideration, i.e. the tank walls are adiabatic. These simplifications are considered to reduce the total number of grid elements in the numerical mesh. The meshes are built up of hexahedral map cells, and the number of grid elements used in the model is 50,975 cells for the 'fine grid' or 'grid-1' which was used in all calculations. Also, two other grid cases are used to compare the results with the fine grid, one of them is a coarse grid which has 15,310 cells while the other is fine also (named 'grid-2') and has 46,715 cells. Figs. 4-a and 4-b illustrate the fine grid faces of the XZ-plane and the XY-plane, respectively. For the coarse grid, faces of the XZ-plane and the XY-plane are shown in Figs. 5-a and 5-b, respectively. The CFD code Fluent 6.1 with the grid generation tool Gambit [8] is used to model the flow in the tank by solving the momentum, turbulence and energy equations. The realizable $k-\varepsilon$ model was used for modeling of the turbulent flow and the buoyancy is modeled using the Boussinesq approximation. Operating temperature $T_{cold} = 293.15\ K$ is used in the buoyancy term, which is the temperature of the cold water.

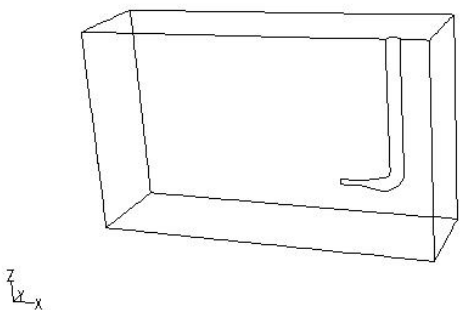

Fig. 3: Model outline of the symmetrical half tank

Because the water inside the tank was at rest before starting the water injection, the initial values of all dependent variables are taken to be zero except the initial temperature which is taken to be 293.15° k.

Numerical solutions are obtained for unsteady flow while pressure, velocity, temperature and turbulence distributions inside the water tank are analyzed. In order to achieve convergence, Under-Relaxation Parameters are used on pressure, velocities, energy, turbulent viscosity, turbulence kinetic energy and turbulent dissipation rate.

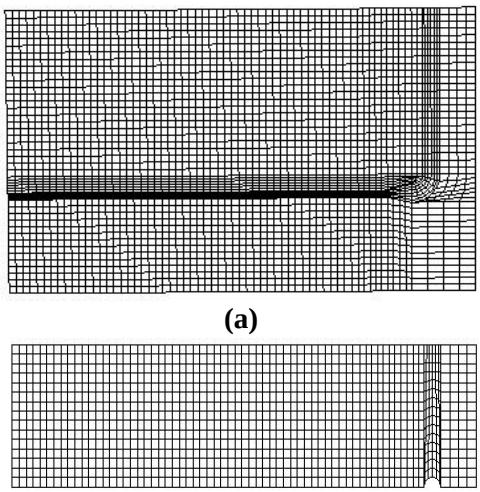

(a)

(b)

Fig. 4: Fine grid of **(a)** a vertical surface (XZ plane), and **(b)** a horizontal surface (XY plane).

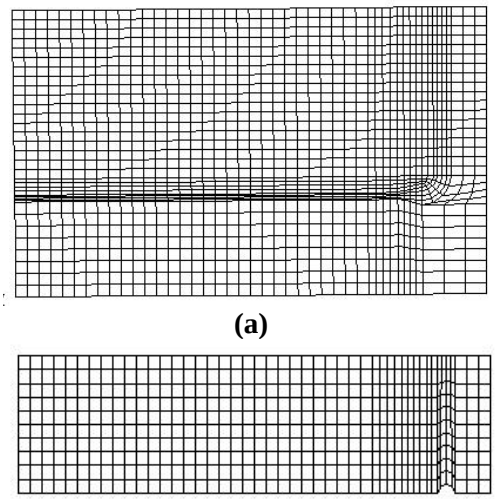

(a)

(b)

Fig. 5: Coarse grid of **(a)** a vertical surface (XZ plane), and **(b)** a vertical surface (XY plane).

Body Force Weighted Discretization is used for pressure and the velocity-pressure coupling is treated using the PISO algorithm with the Skewness-Neighbor Coupling correction parameters. A Second-Order Upwind scheme is used in the equations of momentum, energy, turbulence kinetic energy and turbulence dissipation rate. A 3-D Segregated Implicit Solver with the Implicit Second-Order scheme was used for unsteady formulations. A time step of 0.1 sec was used during the calculations. The heat losses from the tank have not been modeled. The number of iterations which was used in this problem is 100

iterations for each time step. Convergence is achieved for all physical quantities for the three different cases. Fig. 6 shows the residuals of all dependent variables for the first 1000 iterations (t=1 sec) for the first case.

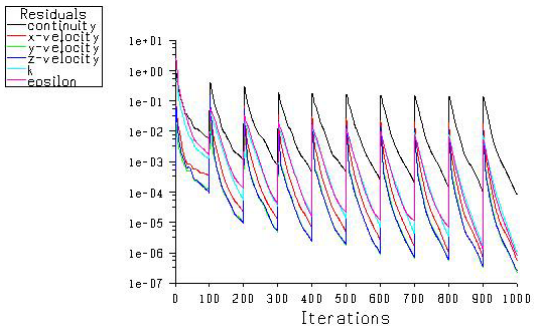

Fig. 6: Residuals of the dependent variables for the first 1000 iterations at t=1 sec for the first case.

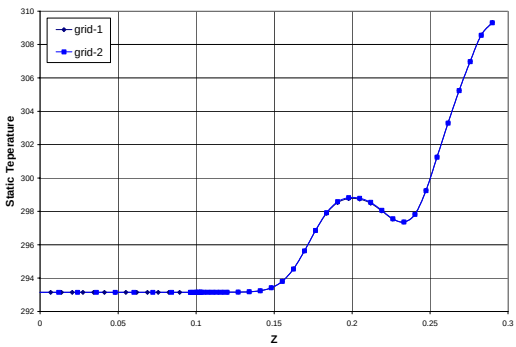

(a)

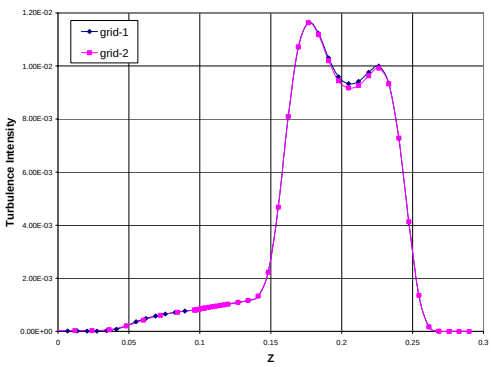

(b)

Fig. 7: (a) static temperature and (b) turbulence intensity profiles as a function of z with different grid size at t=105 sec, for the third case.

In this study we will define two lines one of them parallel the x-axis with the dimensions (x=0.0-0.36, y=0.0001, z=0.1); this line lies in the core of the jet and will denoted by x. The other parallel the z-axis with the dimensions (x=0.1, y=0.0001, z=0.0-0.29) and is close to the wall opposite the jet entrance, is also an important area.

Fig. 7 shows a comparison for the temperature and turbulence intensity, plotted as a function of z, between the two different fine grid sizes 'grid-1' and 'grid-2' as defined above. These figures indicate that the solutions are not depending on the mesh for these cases. Also, Figs. 8(a, b) illustrate a comparison between the fine grid size case and the coarse grid case for the static pressure and static temperature, respectively. From these figures it can be seen that the solutions for the two cases have the same behavior with only small quantitative differences.

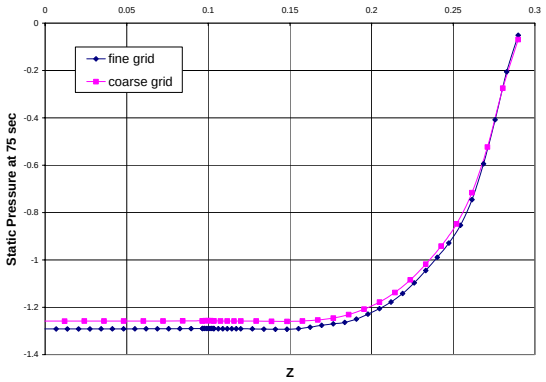

(a)

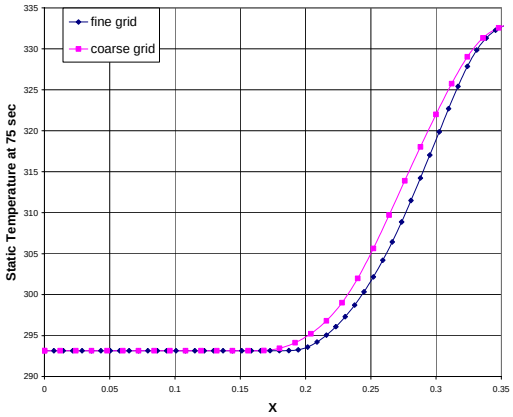

(b)

Fig. 8: (a) static pressure (b) static temperature profiles as a function of x, with different grid size, for the third case.

4 Results and Discussion

Static pressure along of the defined straight line x with various values of the time for the first case $\Delta T = 0$ K is shown in Fig. 9. This figure indicates that the static pressure decreases as time increases along x. Also, it can be seen that the static

pressure in the jet area is greater than it in close to the wall. The area between the inlet and the opposite wall has a small static pressure. It is interesting to note from Fig. 9 that advancing time steps the effect of time on pressure tends to vanish. This means that unsteady-state tends to approach steady-state.

Fig. 10 shows the turbulence intensity profiles as a function of z with various values of time for the first case. It is observed that the highest turbulence intensity lies in the jet area. The top and the down parts of the tank have small turbulence intensity. Time effect on the turbulence intensity is non-uniform depending on the turbulence state inside the tank.

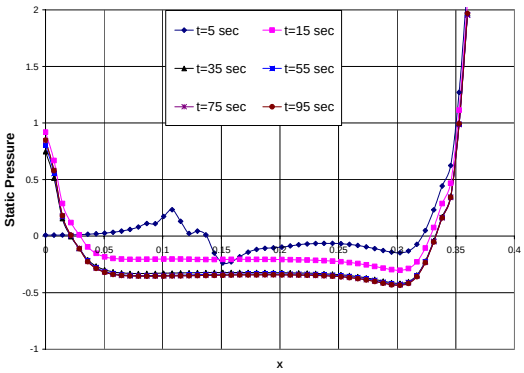

Fig. 9: Static pressure distribution as a function of x, with various values of time, for the first case.

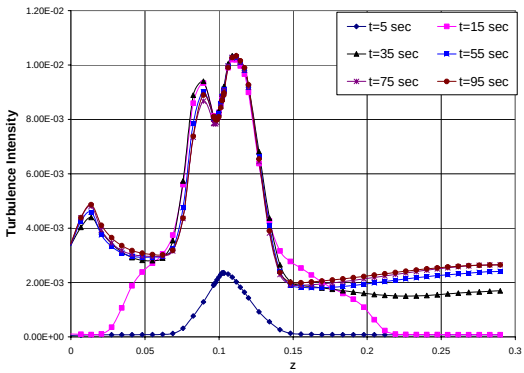

Fig. 10: Turbulence intensity profiles as a function of z, with various values of time, for the first case.

The distribution of the velocity magnitude as a function of z with various values of time for the second case is shown in Fig. 11. It is noteworthy that the middle part (jet area) of the tank has the highest velocity magnitude while it is smaller in the top part and tends to vanish in the bottom part of the tank.

Figure 12 shows the static temperature distribution as a function of z with various values of time for the second case. It is clear that the top part of the tank has the highest temperature and the opposite is true for the bottom part where the temperature seems to be the same as the initial temperature of the tank (293 K). From the same figure it can be seen that the static temperature increases as the time increases.

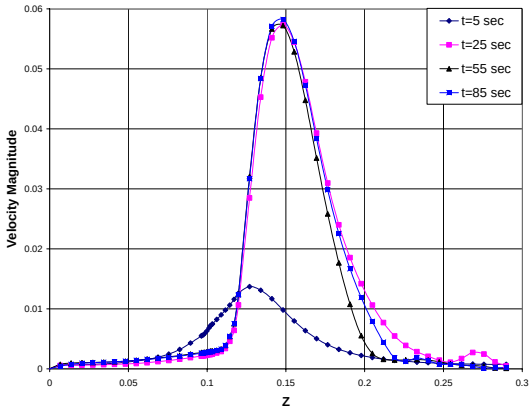

Fig. 11: Velocity magnitude profiles as a function of z, with various values of time, for the second case.

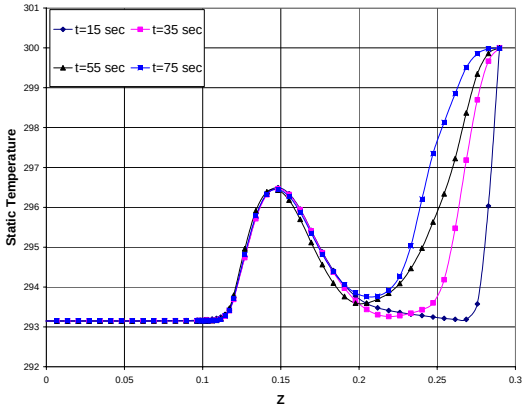

Fig. 12: Static temperature profiles as a function of z, with various values of time, for the second case.

A comparison between the static pressure profiles for the three cases of temperature difference $\Delta T = 0,\ 20,\ 40$ K as a function of x are shown in Fig. 13 at t=85 sec. Fig. 13 shows that the static pressure profiles along the line x decrease as the temperature difference increases, and that the highest pressure for each case lies in the inlet area.
In Figs. 14-a and 14-b the velocity magnitude profiles as a function of x, and z, respectively, are plotted for different temperature differences $\Delta T = 0,\ 20,\ 40$ K at t=85 sec.

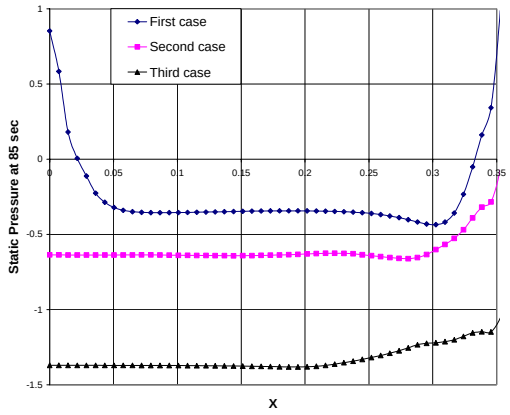

Fig. 13: Static pressure profiles as a function of x, with temperature differences $\Delta T = 0,\ 20, 40\ \ \mathrm{K}$.

Fig. 14-a, indicates that the velocity magnitude along x close to the wall for the first case is higher than for the second and third cases. This because the line x lies in the center of the jet for the first case, while for the second and third cases the position of the jet area lies above x according to buoyancy effect. From Fig. 14-b, it is noteworthy that the position of the highest velocity magnitude depends on the position of the jet area which is shifted by buoyancy force in terms of temperature difference.

The static temperature profiles as a function of z, are shown in Fig. 15 for three temperature differences $\Delta T = 0,\ 20,\ 40\ \ \mathrm{K}$ at t=85 sec. From Fig. 15 it can be seen that the temperature is increased by raising the temperature difference especially in the top of the tank, while, there is no difference at the tank bottom.

Fig. 16 shows the turbulence intensity profiles as a function of z for different temperature difference $\Delta T = 0,\ 20$ and $40\ \ \mathrm{K}$ at t=85 sec. From Fig. 16 one can see that the position of the highest turbulence intensity depends on the temperature difference. The highest turbulence intensity lies in the jet area, thus for the first case, $\Delta T = 0\ \ \mathrm{K}$, in the position around the inlet (because in this case there is no buoyancy force). The position of the highest turbulence intensity of the second case $\Delta T = 20\ \ \mathrm{K}$ lies above the position of the first case, and the position of the highest turbulence intensity of the third case $\Delta T = 40\ \ \mathrm{K}$ lies above the position of the second case.

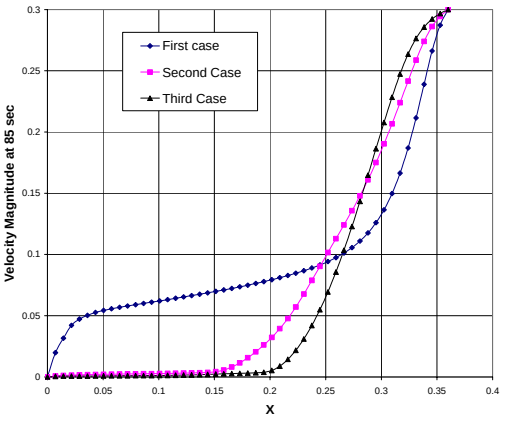

(a)

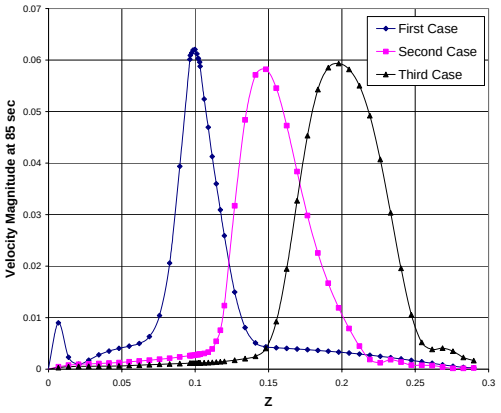

(b)

Fig. 14: Velocity Magnitude profiles as a function of **(a)** x, **(b)** z with different temperature difference.

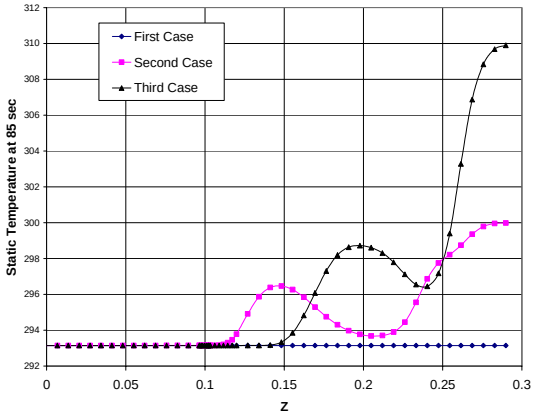

Fig. 15: Static temperature profiles as a function of z for different temperature differences.

Fig. 17 shows the velocity vectors on the parallel vertical XY planes x=0.1, x=0.2, x=0.3 and x=0.4 for the third case, at 85 sec. It is obvious that, the jet area has the highest velocity. After impacting the opposite wall the water returns above and below the jet.

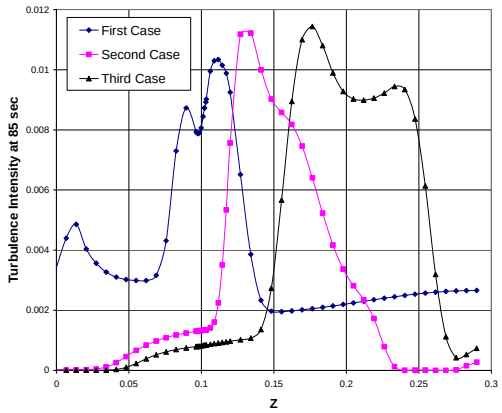

Fig. 16: Turbulence intensity profiles as a function of z for different temperature differences.

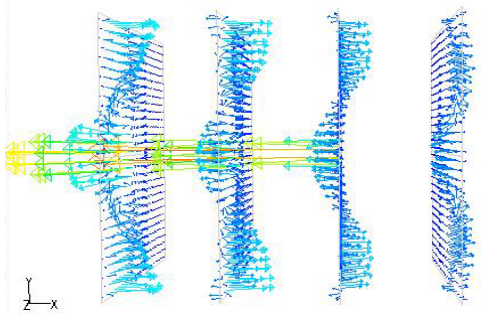

Fig. 17: Velocity vectors in parallel vertical XY plane x=0.1, x=0.2, x=0.3 and x=0.4 for the third case, at 85 sec.

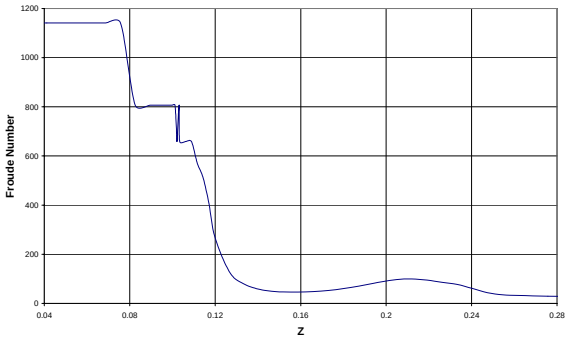

Fig. 18: Internal Froude number as a function of z, for the second case.

The internal Froude number Fr is a dimensionless parameter also known as the Richardson number and defined as $Fr = \sqrt{\rho_0 u^2 / g d_0^2 \Delta\rho}$, where ρ_0 is the reference density, u is the inlet velocity, g is the gravitational accelerate, d_0 is the inlet diameter, and $\Delta\rho$ is the vertical density gradient. The internal Froude number is plotted in Fig. 18 as a function of z, using the polynomial approximation at 85 sec for the second case. Since the Froude number is a kinetic energy divided by the buoyancy force, it has high values in the top part of the tank and low values at the bottom.

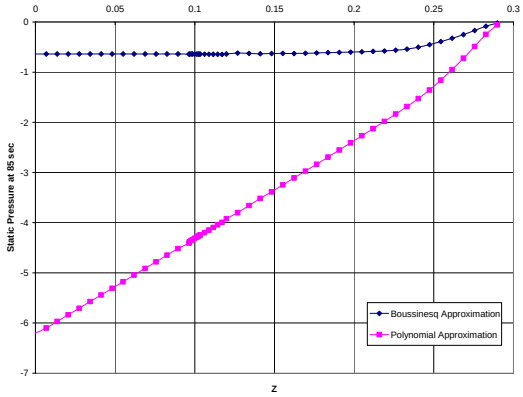

(a)

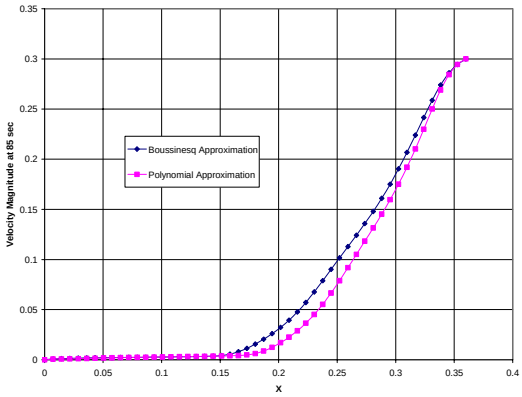

(b)

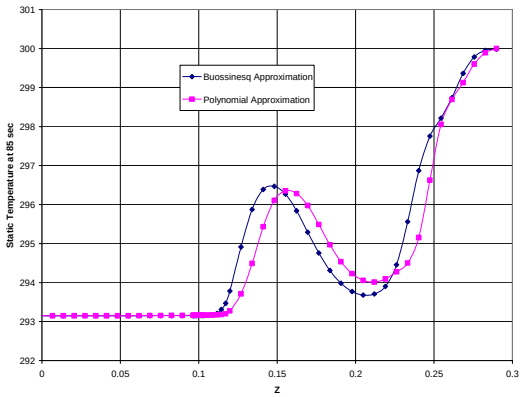

(c)

Fig. 20: Comparison between Boussinesq and polynomial approximation of (a) static pressure (b) velocity magnitude and (c) turbulence intensity distributions for the second case.

4.1 Polynomial approximation

In this section another approximation of the physical properties of water such as density, dynamic viscosity, thermal conductivity and specific heat. They are expressed as functions of temperature using the interpolation method in the temperature range 293.15-313.15 K for the second case:

$$\rho(T) = -18285.1 + 191.8515\,T - 0.63526\,T^2 + 0.0007\,T^3$$
$$c_p(T) = 5813.506 - 10.5941\,T + 0.017143\,T^2 + 2.05\times10^{-13}\,T^3$$
$$K(T) = 4.93680779 - 0.0485048\,T + 0.00017361\,T^2 - 2.0\times10^{-7}\,T^3$$
$$\mu(T) = 0.16522624 - 0.00150221\,T + 4.6\times10^{-6}\,T^2 - 4.73\times10^{-9}\,T^3$$

The purpose of this section is to compare between this approximation and the Boussinesq approximation which is used above as shown in Figs. 20 (a, b, c). The results indicate that the distribution of velocity and temperature turbulence intensity has the same behavior with small quantitative differences for the two approximations, while the behavior of pressure distribution as a function of z is different (see Fig. 19-a). This is because in the Boussinesq approximation density varies only in the buoyancy force term in momentum equation and is considered constant in the other terms, while in the polynomial approximation the density varies always as a function of the temperature. Since the pressure term is divided by density, it should be affected by variation of density, which leads to a more realistic pressure distribution.

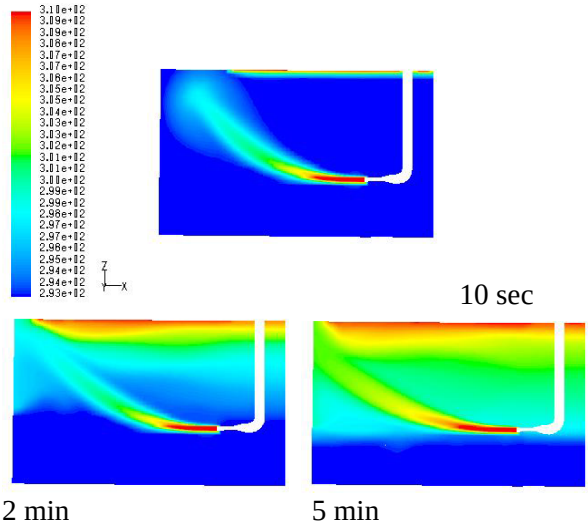

Fig. 20: Contours of the static temperature, for times 10 sec, 1 min and 2 min, various for the third case.

A good prediction of the stratification phenomena is shown in Fig. 20 where contours of the static temperature, with the times 10 sec, 1, 2 min, for the third case are plotted.

Fig. 21(a, b) shows pictures of the experimental visualization, and the contours of the velocity magnitude through a vertical section (the symmetry plane), the horizontal sections z=0.06, z=0.1 and z=0.16, the vertical section x=0.1**,** at 65 sec for the first case and at 75 sec for the third case. These figures provide a complete understanding of jet flow under the current conditions for all cases.

5 Conclusions

Numerical CFD calculations and experimental visualizations for the problem of a hot water jet entering horizontally into a water store containing cold water are performed to illustrate the varying behavior of the thermal conditions in a solar store. Three temperature differences with the corresponding Reynolds numbers are considered. From this work one can conclude that:

-When these problems are treated as unsteady-state problems, after certain time the unsteady-state develops into the steady-state.

-Jet entering the tank at the same temperature results in a regular spread of the jet inside the tank, while entering of a hot jet into the tank make the spread of the jet inside the tank depend on buoyancy forces due to the temperature difference.

-The $k-\varepsilon$ turbulence model is suitable to describe turbulent flow for this kind of problems; the Boussinesq approximation was used to model the buoyancy effect.

-Thermal stratification is verified through the temperature distribution.

-A polynomial approximation for the water properties as functions of temperature was compared to the results with the Boussinesq approximation.

Acknowledgement:
The first author would like to thank the Alexander von Humboldt Foundation, Germany for the fellowship and for supporting of this research. The authors would also like to express their thanks to K. Mohammadi and V. Panthalookaran, for the useful and long discussion, on this problem.

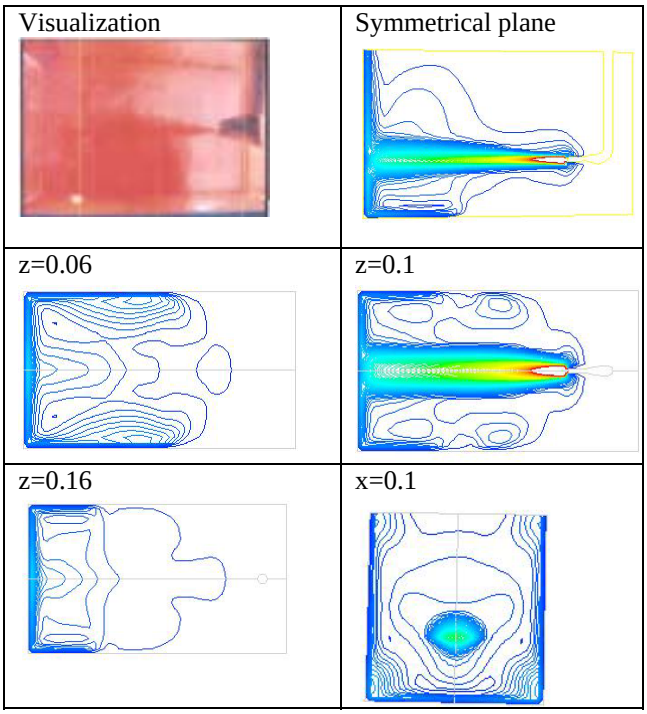

(a)

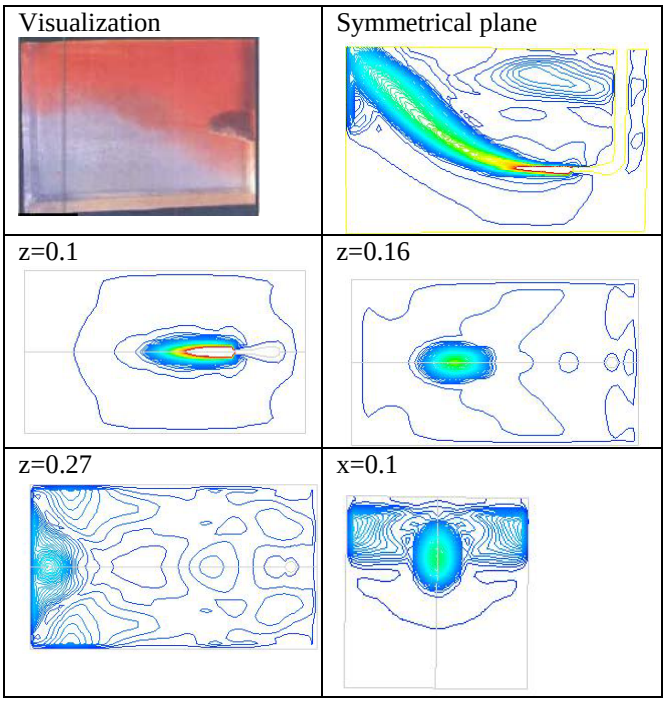

(b)

Fig. 21: Experimental visualization, and contours of the velocity magnitude through horizontal and vertical sections after (a) 65 sec for the first case, (b) 75 sec for the third case.

References:

[1] A. Cabelli, Storage tanks-A numerical experiment, *Solar Energy J*., Vol.19, 1977, pp. 45-57.

[2] S. Knudsen, S. Furbo and L.J. Shah, Design of the inlet to the mantle in a vertical mantle storage tank, *Proc. of ISES 2001 Solar World Congress, Adelaide, South Australia, Nov. 25-Dec. 2.*

[3] L. J. Shah and S. Furbo, Entrance effects in solar storage tanks, *Solar Energy*, Vol. 75, 2003, pp. 337–348.

[4] U. Jordan and S. Furbo, Investigations of the flow into a storage tank by means of advanced experimental and theoretical methods, *ISES Solar World Congress*, June 2003, Goteborg, Sweden.

[5] S. Knudsen, G.L. Morrison, M. Behnia M. and S. Furbo S., Analysis of the flow structure and heat transfer in a vertical mantle heat exchanger, *ISES Solar World Congress*, June2003, Goteborg, Sweden.

[6] T.H. Shih, W.W. Liou, A. Shabbir and J. Zhu, A new $k-\varepsilon$ eddy-viscosity model for high Reynolds number turbulent flows-model development and validation, *Computers Fluids*, vol. 24, no. 3, 1995, pp. 227-238.

[7] W. C. Reynolds, Fundamentals of turbulence for turbulence modeling and simulation, *Lecture Notes for Von Karman Institute Agard Report No. 755*, 1987.

[8] *Fluent 6.1 User's Guide*, Fluent Inc. 2003.